SCIENTIFIC REPORTS

OPEN

SUBJECT AREAS:
ENGINEERING
EVOLUTION

Received
20 May 2014

Accepted
27 November 2014

Published
5 January 2015

Correspondence and requests for materials should be addressed to N.M.P. (nicola.pugno@unitn.it)

Cave spiders choose optimal environmental factors with respect to the generated entropy when laying their cocoon

Eliodoro Chiavazzo[1], Marco Isaia[2], Stefano Mammola[2], Emiliano Lepore[3], Luigi Ventola[1], Pietro Asinari[1] & Nicola Maria Pugno[3,4,5]

[1]Multi-Scale Modeling Lab (SMaLL), Department of Energy, Politecnico di Torino, Corso Duca degli Abruzzi 24, 10129 Torino, Italy, [2]Laboratory of Terrestrial Ecosystems, Department of Life Sciences and Systems Biology, University of Torino, Via Accademia Albertina 13, 10123 Torino, Italy, [3]Laboratory of Bio-inspired & Graphene Nanomechanics, Department of Civil, Environmental and Mechanical Engineering, University of Trento, Via Mesiano 77, 38123 Trento, Italy, [4]Centre of Materials and Microsystems, Bruno Kessler Foundation, Via Santa Croce 77, 38122 Trento, Italy, [5]School of Engineering and Materials Science, Queen Mary University, Mile End Rd, London E1 4NS, UK.

The choice of a suitable area to spiders where to lay eggs is promoted in terms of Darwinian fitness. Despite its importance, the underlying factors behind this key decision are generally poorly understood. Here, we designed a multidisciplinary study based both on *in-field* data and laboratory experiments focusing on the European cave spider *Meta menardi* (Araneae, Tetragnathidae) and aiming at understanding the selective forces driving the female in the choice of the depositional area. Our *in-field* data analysis demonstrated a major role of air velocity and distance from the cave entrance within a particular cave in driving the female choice. This has been interpreted using a model based on the Entropy Generation Minimization - EGM - method, without invoking best fit parameters and thanks to independent lab experiments, thus demonstrating that the female chooses the depositional area according to minimal level of thermo-fluid-dynamic irreversibility. This methodology may pave the way to a novel approach in understanding evolutionary strategies for other living organisms.

The European cave spider *Meta menardi* is preferably found in the twilight zone of most European caves[1]. After mating, females produce a drop-shaped egg sac (cocoon) whose silk has been recently studied[2] underlining its extreme elongation and robustness. The cocoon (2–3 cm in radius) contains an average of 200/300 eggs[3] (Figure 1a–d) and is laid in the nearby of the cave entrance at the end of the summer. After hatching, the spiderlings remain in the cocoon until the first molt, feeding on the yolk[4,5]. They leave the cocoon in spring, move towards the cave entrance[4,6] and disperse via ballooning outside the cave[5,6].

Cocoons avoid the direct exposure of the eggs to the environment, providing protection against predators and parasites, and also from thermal variations[7,8]. In particular, the insulation function of the spider cocoon is documented in literature, demonstrating its resistance to temperature fluctuations and the consequent achievement of an optimal microclimate for the embryological development[9–12].

Although silk properties are extensively studied[13–17], to our knowledge, still little is known on thermal insulation properties of arthropod cocoons as only two scientific papers focusing on this matter have been published up to now[7,18].

The increase of knowledge on the thermo-mechanical properties of natural materials may potentially reveal new insights about the adaptations of species to the environment from an evolutionary perspective. In particular, the investigation of insulation properties of the spider egg sac may contribute in understanding the driving factors at the base of the female choice on the selection of suitable depositional areas in order to increase the survival of the species.

In order to reach this aim, we provide an innovative approach, based on the Entropy Generation Minimization methods[19] originally developed in the realm of engineering sciences. Such approach analyses thermodynamic imperfection stemming from heat transfer, mass transport and fluid flow irreversibility. Owing to the Gouy-

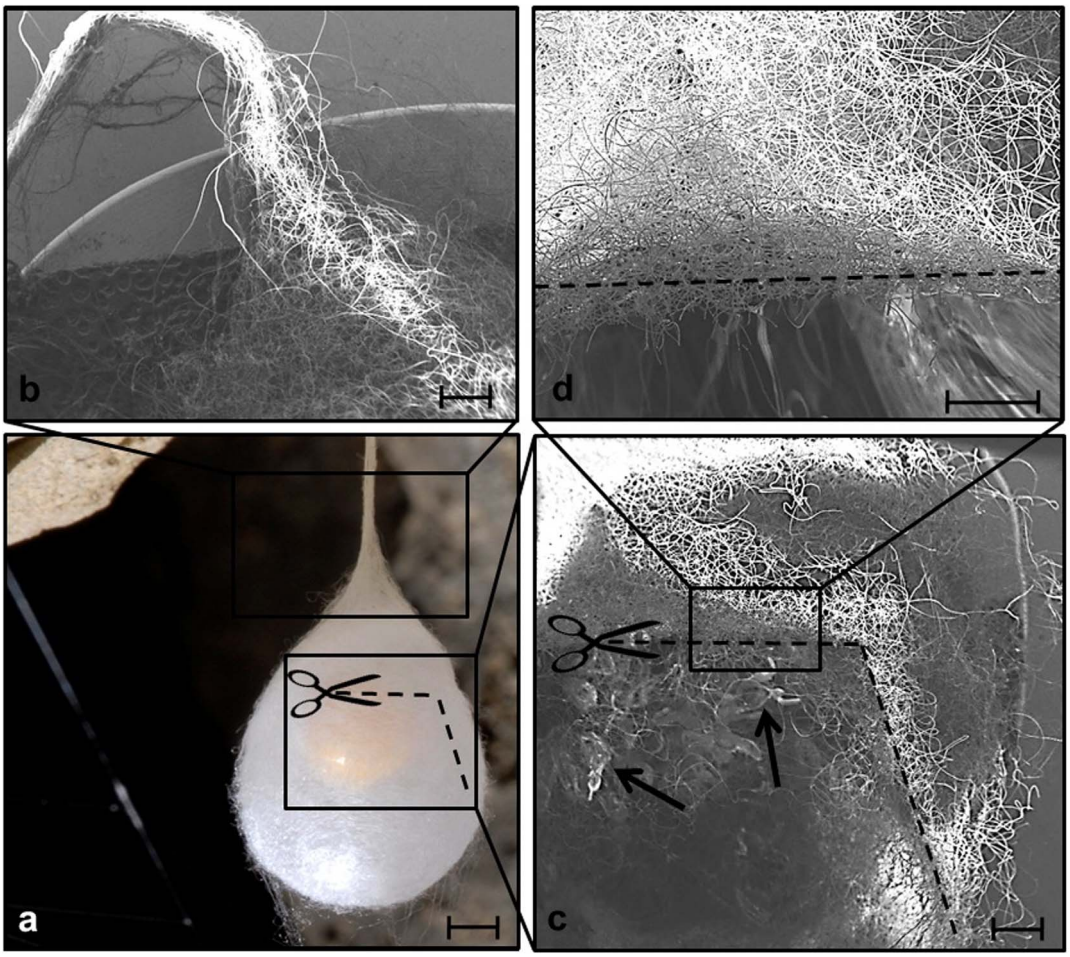

Figure 1 | FESEM characterization of the *Meta menardi* spider cocoon. (a) A cocoon of the European cave spider *Meta menardi*, photo by Francesco Tomasinelli (2009). Scale bar: 5 mm. (b) The upper part and the stalk of the cocoon. Scale bar: 1 mm. (c, d) The walls of the cocoon at different magnifications, scale bars correspond to 1 mm and 500 μm, respectively. The scissors and the black dotted lines indicate cutting of the cocoon wall, which was removed for internal inspection of the cocoon structure and eggs, which are indicated by black arrows.

Stodola theorem, a linear proportionality between the irreversibility level and the more intuitive quantity of useful energy loss (in thermodynamics also known as *exergy* loss) can be proved. As a consequence, design and operation of engineering devices (e.g. heat exchangers, heat pumps) under optimal EGM conditions, imply minimal destruction of useful energy. Ultimately, this leads to a minimal amount of fuel needed for accomplishing a desired task.

The same idea could be referred to a general biological context, in which the fitness of a biological process involving heat transfer, mass transport and fluid flows is maximized when the required energy (i.e. the required amount of food) is minimized. Following similar thermodynamic arguments, Bejan has shown how the optimization of food intake (i.e. useful energy or exergy) can be associated to the optimal size of the organs in animals or to bird flight[19,20].

In this study, we first aim at understanding the influence of the environmental factors on the female preference in laying cocoons under natural conditions (Figure 2a). The considered factors included air flow velocity (below also referred to as air speed), light intensity and distance for the cave entrance. As suggested in literature[4,5,6], the latter seems to be an important factor conditioning the female, given that the cocoon is laid close to the entrance to facilitate the dispersion of the spiderlings outside the cave. However, apart from caves and artificial cavities such as mines, *M. menardi* is able to colonize the shallow air-filled voids of bare rocky debris[21] and other hypogean habitats classified as superficial subterranean habitats (SSH, *sensu*[22,23]). Given the difficulties of studying the SSH without utilizing subterranean traps, we chose the cave environment for our study as a *proxy* of several other habitats that *M. menardi* can occupy.

Moreover, our purpose was to provide evidence that the preference of the female for specific environmental conditions occurring at the depositional areas are those that minimize the amount of global thermo- and fluid-mechanics irreversibility.

Results

In-field study. According to model selection (Table 1), the most appropriate model (see below the corrected Akaike information criterion - AICc) for the available data set had the following structure: $p \sim d + U_{air} + (1|\text{Site})$, where p = probability of presence/absence of cocoon; d = distance from the cave entrance (fixed factor); U_{air} = mean airflow velocity (fixed factor); Site = collection site (random factor).

In the range of the measured values (Figure 3, Table 2), the probability of presence of the cocoon was found to increase significantly in relation to a corresponding increase in the mean airflow velocity [U_{air}: Beta Estimates: 13.506, Standard Error: 6.624, p=0.041 *], reaching 50% around 0.3 m/s and the maximum at 0.6 m/s. Furthermore, the probability of finding a cocoon was also found to increase at minor distances from the cave entrance [d: Beta Estimates: -0.587, Standard Error: 0.324, p=0.070 (*)], however with a weaker effect. The maximum probability was reached very close to the cave entrance and decreased to 50% after 8–10 meters.

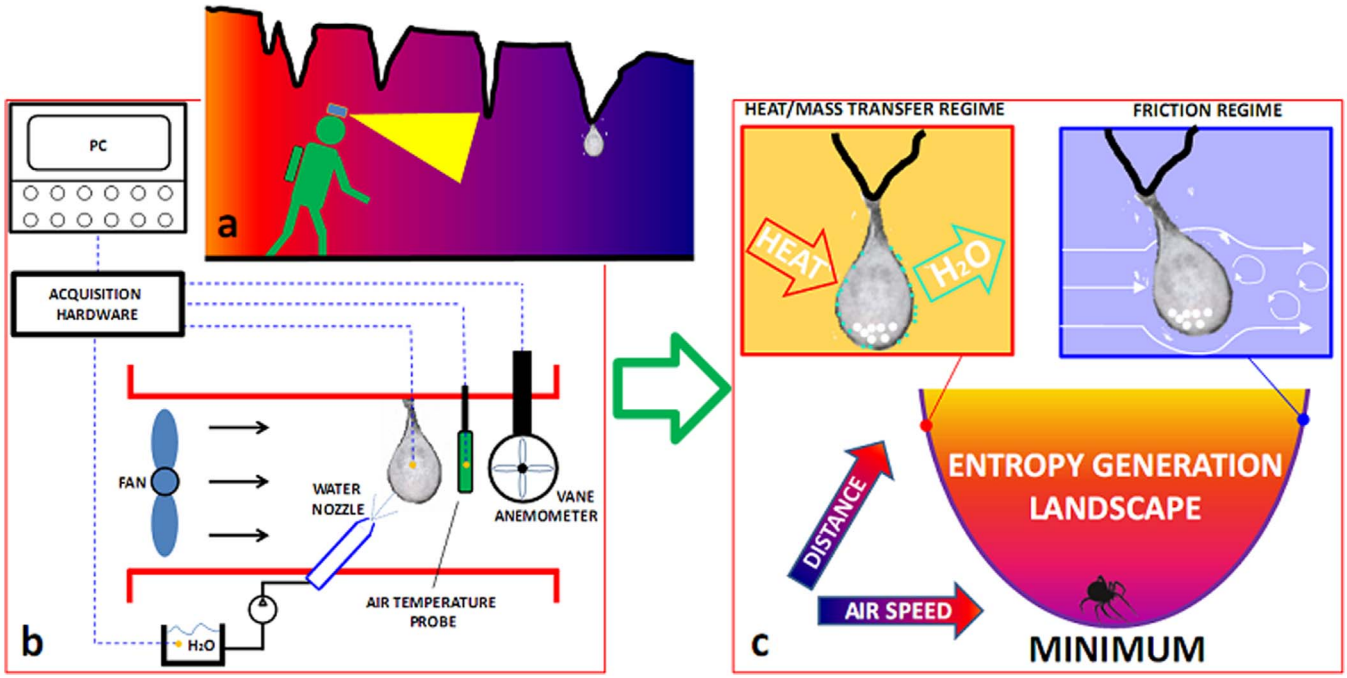

Figure 2 | Summary of the work flow. (a) *in-field* 1-year monitoring and measurements of airflow velocity, distance from cave entrance, presence of the cocoons and final cocoon collecting procedure; (b) laboratory experiments for characterizing the cocoon thermal properties; (c) theoretical modeling based on the EGM method using as input data only the properties measured in phase (b) and direct comparison with observations in phase (a). A relevant agreement is demonstrated without best fit parameters.

Thermal and mass transfer properties of *Meta menardi* cocoon. In a wind channel (sketched in Figure 2b), initial tests were dedicated to the measurements of the thermal transmittance through the cocoon walls as illustrated in detail in the Methods below and the Supplementary Information. The good thermal insulating properties of the cocoon become evident by comparing results referred to as *naked* (i.e. heater not surrounded by a cocoon) with those referred to as *cocoon* (i.e. heater surrounded by a cocoon) in Figure 4a. The latter figure shows that, for vanishing airflow velocities, the transmittance of naked heaters is similar to setups with a cocoon. However, when the airflow velocity increases, the transmittance of the former setup increases as well, attaining (at airflow velocity around 2 m/s) a value three times larger than that observed at zero velocity. On the contrary, the transmittance measured with the cocoon shows a much more moderate increase with the airflow velocity: at 2 m/s, the transmittance with cocoon is less than 50% larger than the corresponding value at 0 m/s.

As a result, the transmittance of the cocoon wall weakly changes with the airflow velocity proving its insulation capabilities. This is mainly due to its porous structure made of many small interstices (see Figure 1a–d), which induce air stagnation at moderately high airflow velocities, even well above the *in-field* recorded velocity: $0.6 < U_{air} < 2$ $[m/s]$.

Results are shown in Figure 4a in terms of physical quantities (namely transmittance as a function of velocity), or converted in terms of dimensionless quantities (namely the Nusselt number *Nu* as a function of the Reynolds number *Re*) in Figure 4b. The latter quantities are often preferred as they allow a more compact form-

Table 1 | Model selection according to corrected Akaike criterion for finite sample size (AICc[37]) ordered from the most to the less appropriate. p = probability of presence/absence of cocoon; U_{air} = mean airflow velocity (fixed factor); d = distance from the cave entrance (fixed factor), L = mean light intensity; Site = collection site (random factor, categorical variable); Df = degrees of freedom; AICc = Corrected Akaike Information Criterion for finite sample size; Wi = Akaike weight

Model structure	Df	AICc	Δ AICc	Wi
$Y \sim U_{air} + d + (1 \mid Site)$	4	29.742	0	0.611
$Y \sim U_{air} + d + L + (1 \mid Site)$	5	31.129	1.386	0.305
$Y \sim d + (1 \mid Site)$	3	35.156	5.414	0.041
$Y \sim d + L + (1 \mid Site)$	4	36.653	6.911	0.019
$Y \sim L + d$	3	38.297	8.554	0.008
$Y \sim d$	2	38.864	9.121	0.006
$Y \sim L + U_{air} + d$	4	39.276	9.534	0.005
$Y \sim d + U_{air}$	3	40.144	10.401	0.003
$Y \sim U_{air} + (1 \mid Site)$	3	44.854	15.111	0
$Y \sim U_{air} + L + (1 \mid Site)$	4	47.051	17.309	0
$Y \sim L + (1 \mid Site)$	3	55.692	25.949	0
$Y \sim U_{air}$	2	55.883	26.141	0
$Y \sim L + U_{air}$	3	56.977	27.235	0
$Y \sim L$	2	58.440	28.697	0

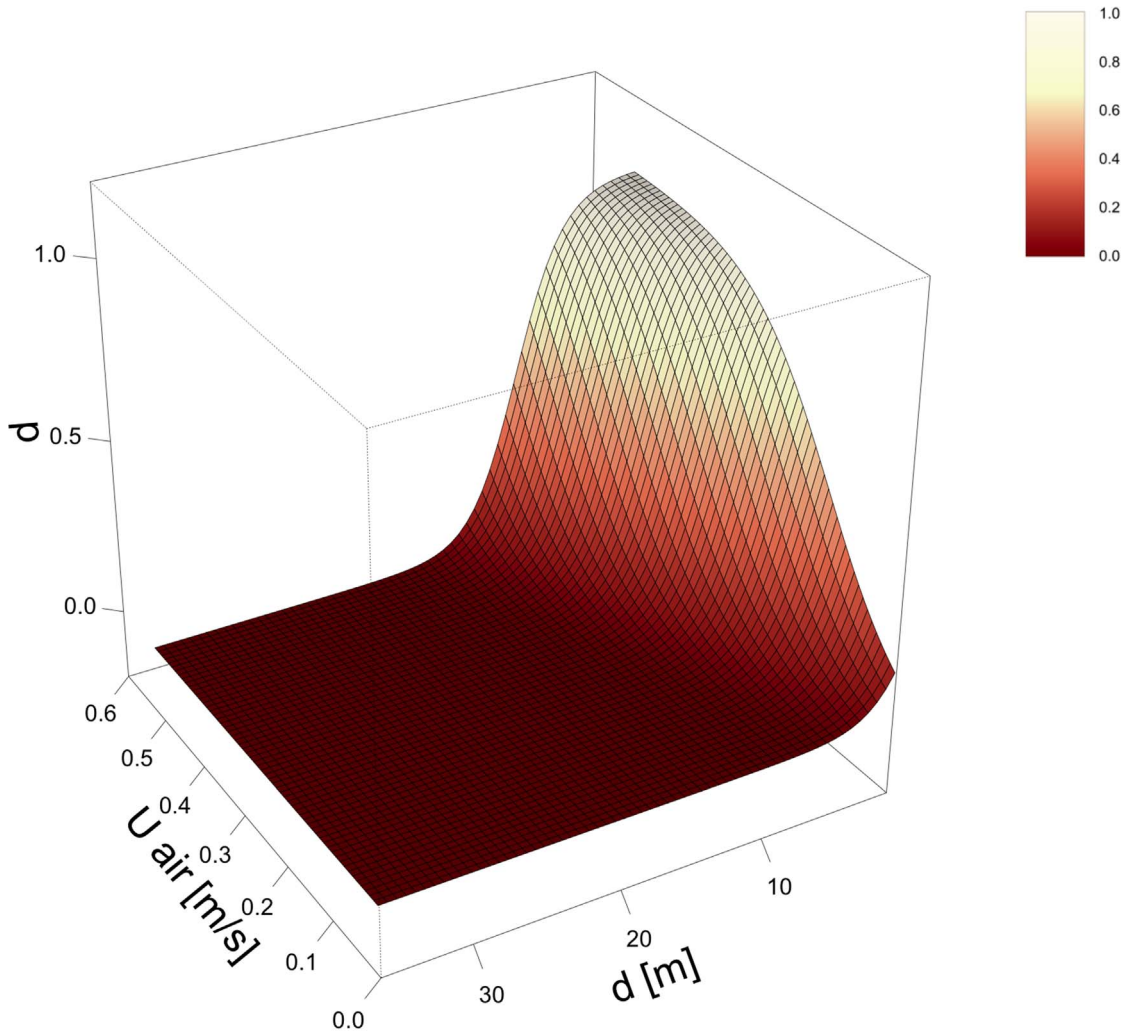

Figure 3 | The binomial Generalized Linear Mixed Model (GLMM). Probability surface shows the relation among mean airflow velocity, distance from the cave entrance and probability of presence of the cocoon of *Meta menardi*, obtained by the binomial GLMM applied to the *in-field* collected data.

alism (e.g. no need to account for the heater size). In the Supplementary Information, we have reported more details on the translation of the physical quantities into the corresponding dimensionless variables. Moreover, relying upon the Chilton-Colburn analogy between heat and mass transfer, we were able to express the analytic dependency of both thermal Tr and mass K transmittances on the velocity value U_{air} (see Supplementary Information). As reported in Figure 4c, those functions were expressed in the following explicit form:

$$Tr = Tr_0 + Tr_1 U_{air}^{\alpha}; \quad K = K_0 + K_1 U_{air}^{\alpha}, \tag{1}$$

with Tr_0, Tr_1, K_0, K_1 and α being appropriately chosen in order to best fit the experimental data. Finally, the characteristic drying time was also investigated and expressed as a function of the airflow velocity $\tau = \tau(U_{air})$ (see Figure 4d).

The above formulas $Tr(U_{air})$, $K(U_{air})$ and $\tau(U_{air})$ were all utilized to explicitly write the total generated entropy functional S_{tot} and the corresponding probability p of cocoon deposition in terms of the airflow velocity and the distance from the cave entrance as derived in detail in the Methods section below:

$$S_{tot} = S_{tot}(U_{air}, d); \quad \mathrm{p} = \exp\left[-(S_{tot} - S_{tot}^{\min})/S_0\right]. \tag{2}$$

with $S_{tot}^{\min}$ and S_0 constants. Iso-level curves of both the generated entropy and deposition probability have been shown in Figure 5, where we also reported the results of the 48 *in-field* observations. Cocoon presence probability is in good accordance with the computed function p, thus supporting our preliminary assumption that the preferred environmental factors are those ensuring minimal production of entropy. In particular, the entropic model predicts the highest presence of cocoons at $U_{air} \approx 0.55$ m/s and low values of d.

Table 2 | Results of the Binomial GLMM applied to *in-field* data (Random effect variance: Site = 4 groups, Variance 6.57, Std. dev. 2.563)

Variable	Beta Estimate	Std. Error	z value	Pr(>|z|)
(Intercept)	−1.430	2.118	−0.68	0.500
U_{air}	13.506	6.624	2.04	0.041 *
d	−0.587	0.324	−1.81	0.070 (*)

Discussion

According to the Gouy-Stodola theorem[24] a linear proportionality between the irreversibility level and the energy loss can be proved. Ultimately, low irreversibility levels could be related to lower amount of primary energy (i.e. fuel in engineering devices or food in animals) needed for accomplishing a desired task. This same idea has been applied to complex systems such as living organisms[19,20].

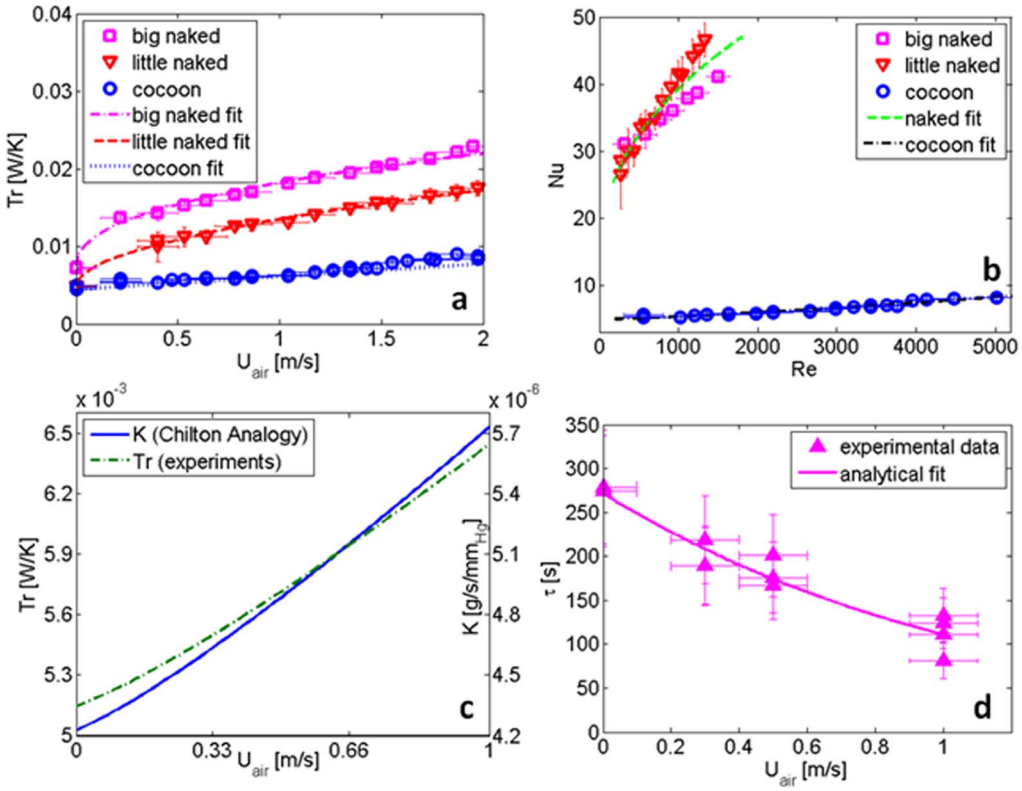

Figure 4 | Experimental results from laboratory tests comparing different setups: naked with BH (big heater), naked with SH (small heater), BH within cocoon, SH within cocoon. (a) Transmittance as a function of the airflow velocity U_{air}. Points refer to experimental data, while lines denote best-fitting curves. (b) Nusselt number as function of Reynolds number. Points refer to experimental data, while continuous lines indicate best fitting curves. (c) Thermal and mass transport transmittances Tr and K as a function of the airflow velocity based on the laboratory experiments. (d) The characteristic drying time τ as function of the airflow velocity U_{air}. Triangles are the experimental points, while continuous line is the corresponding best fitting curve.

In this study, we applied these concepts to study the adaptive significance of the female preference for specific environmental conditions. According to the results of our *in-field* study, the European cave spider *Meta menardi* selects suitable areas for the deposition of the egg sac on the basis of two environmental variables, namely airflow velocity and the distance from the cave entrance within a particular cave. The preferred conditions are found where the air flow velocity ranges between 0.3 and 0.6 m/s within 8–10 meters from the cave entrance. It appears likely that this preference is related to the peculiarity of the life cycle of the spider, in particular to the maintenance of an optimal microclimate for the development of the eggs and to facilitate the migration of spiderlings outside the cave (i.e. dispersion). Moreover, on the basis of a thermodynamic optimization argument, we have observed that such optimal values of those two environmental variables correspond to minimal level of irreversibility. Thermodynamic optimization has been conducted by the EGM method[19,24,25], which has the merit of providing a scalar function S_{tot} (see Methods below) to consistently combine in a unique formula several physically non-homogeneous contributions to total irreversibility.

According to the entropic argument, three main irreversibility sources have been considered in our study: i) Fluid dynamics friction (below denoted by S_{drag} and S_{mov}); ii) Mass transport (S_{mass}); iii) Heat transfer (S_{heat}). From the biological standpoint, an increase of fluid dynamic irreversibility plays a twofold undesired role. First, this is responsible for the corresponding increase in the metabolic energy spent by spiderlings while exiting the cave (i.e. the larger the distance d the larger the amount of required energy). It was observed that once the yolk sac has been consumed, the spiderlings usually do not feed until they disperse outside[5]. Indeed, a large percentage of spiderlings of *M. menardi* emerging from cocoons displays a strong positive

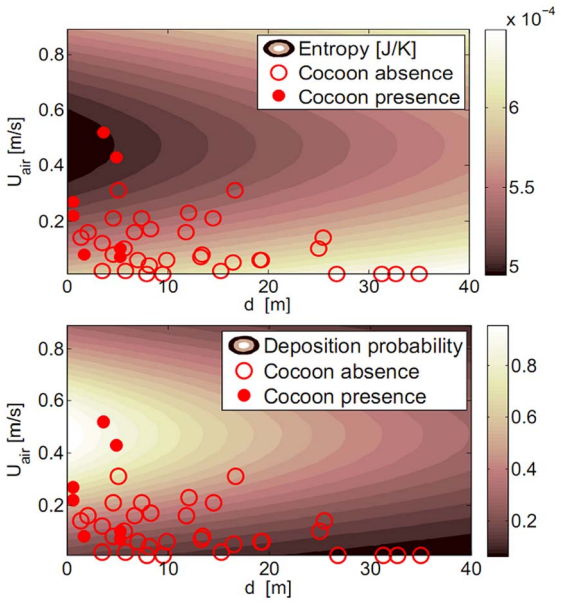

Figure 5 | Entropy isocontours. (a) Isocontours of the total generated entropy according to equation (15) corresponding to: $\phi = 0.65$, $D_c = 1.8$ cm, $T_a = 15°C$, $D_s = 6$ mm, $U_{spider} = 0.4$ m/s, $N_{spider} = 250$ (see ref. 28). (b) Cocoon deposition probability by equation (16) is reported with a reference entropy of $S_0 = S_{tot}^{min}/8$. *In-field* experimental data are also reported with disks and circles denoting presence and absence of cocoon, respectively.

Table 3 | List of the study sites with the total number of plots considered for the *in-field* study and number of observed cocoons for each cave during the survey, dates of deposition and hatching. The cocoons tested in the laboratory were taken in Grotta del Bandito in October 2013

Cave name	Cadastre number	Type	Municipality	Province	N° of plots	N° of cocoons	Deposition	Hatching
Grotta del Bandito	1002 Pi/CN	Natural cave	Roaschia	CN	16	1	Aug 2012	March 2013
Cave di Marra	Art. Pi/TO	Abandoned mine	Villar Focchiardo	TO	22	11	Aug/Sep 2012	Feb/March 2013
Balma Fumarella	1597 Pi/TO	Natural cave	Gravere	TO	10	2	Aug 2012	Feb/March 2013

phototaxis[6], moving away from the cocoon towards the light of the cave entrance[4,5]. In the absence of food intake, it appears likely that the vicinity of the cocoon to the cave entrance minimizes the amount of energy necessary to the spiderlings to accomplish this migration, thus maximizing the reproductive success of the species. On the other hand, the vicinity to the cave entrance may excessively expose the cocoon to a higher predation risk (i.e. by parasitoids coming from the outside, see Ref. 26). In this respect, the external layer of the cocoon has been proved to ensure protection from external attacks[2,27]. Here it is worth to stress out that the distance from the cave entrance has to be considered with caution. Indeed, the distance from the entrance itself can be regarded as a surrogate of several other environmental and microclimatic conditions, for instance light intensity and air velocity (i.e. microclimatic variability)[28]. However, our statistical approach deals with this problem via the analysis of collinearity among the covariates and the model selection, aiming to disentangle the effects provided by different covariates on the dependent variable[29,30]. In particular, light intensity and the distance from entrance were not correlated (given the morphology of the cave, both dark and illuminated plots occurred both near and far from the cave entrance). A similar trend was found for all other combinations of variables. In addition, despite the inclusion in the model of an array of covariates, model selection pointed out a significant effect of the distance from entrance *per se* (Tab. 1), which we interpreted as a factor facilitating the spatial migration of the spiderlings.

A second aspect also included in our thermodynamic model is related to microclimatic conditions at the surface of and within the cocoon. To this respect, fluid dynamic irreversibility (i.e. friction between flowing air and a cocoon) should be minimized as it provides an excess of heat to the cocoon thus altering the internal climatic conditions and possibly the development of the eggs[31]. Heat can be generated by the friction forces between air and the cocoon wall as well as by egg scrubbing.

Similarly, a minimal level of irreversibility generated during water mass and heat transfer is also desirable as this ensures small time-averaged temperature difference and water pressure difference between the cocoon and the environment. Under these conditions (i.e. short temperature and pressure differences regime), the drying process is only experienced for short time thus minimally affecting the microclimatic conditions within the cocoon.

On the contrary, at higher airflow velocity, higher friction generates heat thus altering the optimal conditions within the cocoon. Moreover, if from one side lower air velocity minimizes friction, on the other it may result in lower drying effect thus leading to an excessive wetting of the cocoon. Inside the cave and other hypogean habitats colonized by *M. menardi* (see, e.g., Ref. 21), the relative humidity is very high, usually showing partial or complete saturation[22,32]. The cocoon can potentially get wet via the running water that often flows over the internal surfaces of subterranean chambers or by the condensation of water droplets over the cocoon external layer when the water content in the cave air is above the saturation. Since the cocoon is suspended from the chamber ceiling by a stalk of silk, it is most often kept away from the running water on the walls[5]. On the other hand, the wetting of the cave surfaces (and thus of the cocoon) through the deposition of water from the atmosphere is by no means an extraordinary event[31]. Under such condition, the cocoon could grow heavy and collapse as well as become a suitable substrate for fungal attacks[5]. By drying the cocoon, the presence of a flow of air may limit this negative effect connected with the humidity.

In the light of the above considerations, the total irreversibility level S_{tot} can be interpreted as an overall measure of two phenomena: i) the unsuccessful egg development due to unsuitable microclimatic conditions; ii) the unsuccessful migration of the spiderlings toward the entrance due to a large required metabolic energy. In evolutionary terms, the ecological conditions selected by the female in the deposition area ensure a higher reproductive success and thus are promoted in terms of Darwinian fitness.

Moreover, considering the experimental results for the related cocoon thermal properties and the EGM method reported here, the best conditions for the cocoon deposition are found at the same conditions highlighted in the *in-field* study.

The multidisciplinary approach of combining *in-field* ecological study with the thermodynamic arguments, here proposed, may pave the way to a novel understanding of evolutionary strategies for other living organisms.

Methods

***In-field* study.** In order to study the influence of specific environmental conditions on the female preference for laying the cocoon, we monitored monthly three natural populations of *Meta menardi* occurring in three subterranean sites in the Western Italian Alps, NW-Italy (Table 3 and the Supplementary Information).

We defined forty-eight plots (squared areas of 1×1 m^2, Table 3) that were monitored monthly for one year, from April 2012 to March 2013 (12 total surveys). Plots were randomly placed inside the cave within the natural range of occurrence of adult female spiders (1–40 m), derived from previous observations in the sites[33].

The distance from the cave entrance (d) of each plot was measured at the first survey. During each survey, we registered presence/absence of cocoons and measured light intensity (lux) (L) and airflow velocity (m/s) (U_{air}) (median value of four measurements per plot). For light intensity and airflow velocity we used a portable meter (DO 9847 Delta OHM S.r.l.) equipped with a photometric probe (LP 471 Phot) and a hot-wire probe (AP 471 S1).

During the survey, an amount of fourteen cocoons was laid almost simultaneously in the three study sites in August/September 2012 and hatched in February/March 2013 (Table 3). Data of airflow velocity and light intensity gathered between the deposition and the hatching of the eggs (8 surveys) were pooled in one value by calculating the mean of the registered variables (48 total mean observations).

Data exploration was carried out following[29]. Presence/absence of cocoon was related to the three explanatory variables via a generalized linear mixed model procedure (GLMMs[32]) in R environment[34]. The mixed procedure allowed us to deal with the spatial dependence of the plots, so we included the spatial factor "site" (namely the three subterranean systems in which the plots were located) as a random factor. The Bernoulli distribution was chosen, the response variable containing zeros (absence) and ones (presence). Considering the unbalanced set of zeros and ones in our dataset (14 ones versus 34 zeros), we used the complementary log-log link function (clog-log) as recommended by Ref. 30. The clog-log regression model was fitted via the glmmAMDB[35] R package (version 0.7.7). The outcome of the models consisted of regression coefficients for the explanatory variables, whose significance was assessed via Wald tests[36]. We performed model selection by a stepwise selection procedure, according to AICc (corrected Akaike information criterion[37]) that is appropriate when the number of observations is small[38]. The AICc values were calculated via the MuMIn[39] R package (version 1.9.13). The model validation was carried out following[30] (See Supplementary Information).

FESEM characterization of the *Meta menardi* spider cocoon. The cocoon walls were cut leaving an opening (see black dotted lines in Figure 1a) in order to scan the wall structure using the Field Emission scanning electron microscope (FESEM, FEI-InspectTM F50, at 1–2 kV) equipped with a field emission tungsten cathode. These have been fixed to aluminium stubs by double-sided adhesive carbon conductive tape (Nisshin EM Co. Ltd.). Samples were used as collected, no fixation processes were made to avoid any alteration of the cocoon structure[40,41].

Characterization of thermal and mass transport properties of *Meta menardi* cocoons. For assessing thermal and mass transport performances of *Meta menardi* cocoons, we performed several experimental tests by introducing an electrical heater inside the cocoon along with a thermocouple in contact with the above heater. This enabled us to have an estimate of the temperature T_w inside the egg sac at a given thermal power and external fluid-dynamic conditions.

To ensure a homogeneous temperature distribution, the thermocouple and the heater were wrapped together in an aluminum foil and a good thermal contact was ensured by a thin layer of thermal interface compound (with thermal conductivity larger than 2 W/K/m).

This assembly was introduced inside the cocoon, which was placed on the symmetry axis of the wind channel, whose dimensions are $10 \times 10 \times 40$ cm^3 (with a cross section of 10×10 cm^2). At the channel inlet, an adjustable velocity fan induced an air stream around the cocoon, thus mimicking the action of wind under natural conditions. An additional thermocouple measured the ambient air temperature T_a in the center of channel middle section.

A hydraulic characterization of the wind channel has been performed before measurements. Namely, using a vane anemometer placed at the center of the wind channel (see also Figure 2b), a characteristic curve has been constructed by recording the electrical power supplied to the fan corresponding to a measured air speed. The latter curve has been used subsequently in the experiments for inferring the air speed value at a given voltage supplied to the fan.

Two different heaters have been utilized in order to investigate possible size effects. The first heater was characterized by a bigger size and smaller electrical resistance (referred to as big heater-BH). The second heater presented a smaller size and a larger electrical resistance (referred to as small heater - SH). The big (small) heater had a cylindrical geometry with height, diameter and resistance of 22.2 mm (10.4 mm), 5.05 mm (4.15 mm) and 22.4 Ohm (98.9 Ohm), respectively.

Evaluation of total irreversibility and cocoon deposition probability. We considered wetting and adiabatic cooling as sufficiently fast processes (compared to the subsequent drying phenomenon), so that starting from t_{start}, the phenomenon of interest was approximated by a sudden cooling with $\Delta T_{\max} = T_a - (T_w)_{\min} = \Delta T_{\max}$ followed by a first-order exponential decay with characteristic time τ. Upon the choice of the relative humidity φ and the ambient temperature T_a, $\Delta T_{\max}$ is dictated by the corresponding wet bulb temperature T_{wb}: $\Delta T_{\max} = T_a - T_{wb}$, which was computed by the following empirical correlation[42]:

$$T_{wb} = (T_a - 273)\left[0.45 + 0.6\varphi\left(\frac{p}{1060}\right)^2\right] + 273, \tag{3}$$

with temperatures expressed in Kelvin, and pressure p in hPa (0.1 kPa).

During the drying process of a cocoon under forced air convection, mainly three phenomena contribute to the generation of entropy: i) fluid-dynamic drag; ii) heat transfer under finite temperature differences; iii) mass transfer under finite pressure differences. Following a similar argument as in Ref. 24, we can quantify the above three contributions to the entropy production (during the drying process) as follows:

$$\dot{S}_{drag} = \frac{F_D U_{air}}{T_a}, \quad \dot{S}_{heat} = \frac{Tr(T_w - T_a)^2}{T_a T_w}, \quad \dot{S}_{mass} = \frac{K[p_s(T_w) - \varphi p_s(T_a)]^2}{\rho_a T_a}, \tag{4}$$

with ρ_a and F_D denoting the air density and the drag force. Under the assumption of spherical cocoon, the latter force can be estimated as:

$$F_D = \frac{C_D \rho_a \pi D_c^2 U_{air}^2}{8}, \tag{5}$$

where D_C is the cocoon diameter and the drag coefficient C_D is computed by means of the well-known correlations[43]:

$$C_D = \frac{24}{\mathrm{Re}}\left[1 + 0.1315\mathrm{Re}^{0.82 - 0.05w}\right] \text{ if } \mathrm{Re} \le 20, \tag{6}$$

$$C_D = \frac{24}{\mathrm{Re}}\left[1 + 0.1935\mathrm{Re}^{0.6305}\right] \text{ if } 20 < \mathrm{Re} \le 260, \tag{7}$$

$$\log_{10} C_D = 1.6435 - 1.1242w + 0.1558w^2 \text{ if } 260 < \mathrm{Re} \le 1.5 \times 10^3, \tag{8}$$

with the Reynolds number $\mathrm{Re} = D_c U_{air} \rho_a / \mu$ and $w = \log_{10}(\mathrm{Re})$. The dependence of the saturation pressure on the temperature $p_s(T)$ in equation (4) is accounted by means of a fourth order polynomial as follows:

$$p_s(T) = c_1 T^4 + c_2 T^3 + c_3 T^2 + c_4 T + c_5, \tag{9}$$

where pressure is expressed in Pa, temperatures in Kelvin, $c_1 = 0.000965$, $c_2 = -1.087$, $c_3 = 462.3$, $c_4 = -8.789 \times 10^4$ and $c_5 = 6.297 \times 10^6$.

During the drying process, the above three sources of irreversibility are responsible of a total entropy production which amounts to:

$$S_{drying} = \int_0^{\Delta t} \dot{S}_{drag} dt + \int_0^{\Delta t} \dot{S}_{heat} dt + \int_0^{\Delta t} \dot{S}_{mass} dt, \tag{10}$$

where Δt is a proper multiple of the characteristic time τ (i.e. $\Delta t \approx 3\tau$), after which the cocoon can be practically considered at thermal equilibrium with the environment. In the following, we focus on a single event during which the cocoon external surface gets fully wet.

The total entropy produced during the drying process can be explicitly expressed as a function of the airflow velocity U_{air} substituting the experimental functions $Tr(U_{air})$, $K(U_{air})$ and $\tau(U_{air})$ plotted in Figure 4c, d in the equations (4):

$$S_{drying} = S_{drying}(U_{air}). \tag{11}$$

Furthermore, the length d is responsible of additional entropy production $\dot{S}_{mov}$ due to the friction generated during the movement of the young spiders while trying to exit the cave. In the following, we report the simplest way of estimating such a contribution:

$$\dot{S}_{mov} = N_{spider} \frac{F_S U_{spider}}{T_a}, \tag{12}$$

where N_{spider}, F_S and U_{spider} are the number of spiders exiting the cocoon, a friction force associated with the spider movement and the traveling speed at which spiders move, respectively.

An estimate of the drag force can be obtained by equation (5): $F_S = F_D$ (upon the choice of a characteristic dimension of the young spiders D_s), while the total amount of entropy generated during the travel from the cocoon to the cave entrance is:

$$S_{mov} = \int_0^{d/U_{spider}} N_{spider} \frac{F_D U_{spider}}{T_a} dt = N_{spider} \frac{F_D d}{T_a}, \tag{13}$$

which, as opposed to equation (11), depends on d: $S_{mov} = S_{mov}(d)$. It is worth noticing that here, for simplicity and without loss of generality, we only consider fluid-dynamic friction and neglect the contribution due for instance to other forms of dissipation, e.g. friction developed while the spider moves upon the cave walls (named F_{SC}). In case of knowledge of F_{SC}, equation (13) can be more accurately expressed as:

$$S_{mov} = N_{spider}(F_D + F_{SC})d / T_a. \tag{14}$$

According to EGM, optimal deposition conditions are found at the minimum of the following functional:

$$S_{tot} = S_{tot}(U_{air}, d) = S_{drying}(U_{air}) + S_{mov}(d). \tag{15}$$

The above expression is valid under the assumption that the amount of entropy (11) produced during a single complete wetting and subsequent drying process incorporates the entire amount of total irreversibility during the entire life of a single cocoon (see also the Supplementary Information).

Finally, according to classical thermodynamics, we assumed the following exponential relationship between the cocoon deposition probability p and entropy S_{tot}:

$$\mathrm{p} = \exp\left[-\left(S_{tot} - S_{tot}^{\min}\right)/S_0\right], \tag{16}$$

where $S_{tot}^{\min}$ is the absolute minimum value of the functional (15), while $S_0 \propto S_{tot}^{\min}$ is a proper reference entropy.

1. Nentwig, W., Blick, T., Gloor, D., Hänggi, A. & Kropf, C. *Spiders of Europe.* (2013) Available at: http://www.araneae.unibe.ch/. (Accessed: 29th April 2014).
2. Lepore, E., Marchioro, A., Isaia, M., Buehler, M. J. & Pugno, N. M. Evidence of the most stretchable egg sac silk stalk of the European spider of the year *Meta menardi*. *PLoS ONE* **7**, e30500 (2012).
3. Hörweg, C., Blick, T. & Zaenker, S. The large cave spider *Meta menardi* (Araneae: Tetragnathidae), spider of the year 2012. *Arachnologische Mitteilungen* **42**, 62–64 (2011).
4. Tercafs, R. Nesting dispersal in a cave spider. *Mem. Biospeleol.* **15**, 45–48 (1988).
5. Smithers, P. The early life history and dispersal of the cave spider *Meta menardi* (Latreille, 1804) (Araneae: Tetragnathidae). *Bull. Br. Arachnol. Soc.* **13**, 213–216 (2005).
6. Smithers, P. & Fox Smith, M. Observations on the behaviour of second instars of the cave spider *Meta menardi* (Latreille, 1804). *Newsl. Br. Arachnol. Soc.* **81**, 4–5 (1998).
7. Hieber, C. S. The "insulation" layer in the cocoons of *Argiope aurantia* (Araneae: Araneidae). *J. Therm. Biol.* **10**, 3, 171–175 (1985).
8. McCook, H. C. *American spiders and their spinning work* (Academy of Natural Science, Philadelphia,1890).
9. Kaston, B. J. *Spiders of Connecticut.* [State geological & natural history survey] (Hartford, Conn, 1948).
10. Turnbull, A. L. Ecology of the true spiders (Araneomorphae). *Annu. Rev. Entomol.* **18**, 305–348 (1973).
11. Gertsch, W. J. *American Spiders* [2nd ed.] [274] (Van Nostrand Reinhold Company, New York, 1979).
12. Schaefer, M. An analysis of diapause and resistance in the egg stage of *Floronia bucculenta* (Araneae: Linyphiidae). *Oecologia* **25**, 155–174 (1976).
13. Shao, Z. & Vollrath, F. Surprising strength of silkworm silk. *Nature* **418**, 741 (2002).
14. Jin, H. J. & Kaplan, D. L. Mechanism of silk processing in insects and spiders. *Nature* **424**, 1057–1061 (2003).
15. Altman, G. H. *et al.* Silk-based biomaterials. *Biomaterials* **24**, 401–416 (2003).

16. Cranford, S. W., Tarakanova, A., Pugno, N. M. & Buehler, M. J. Nonlinear material behaviour of spider silk yields robust webs. *Nature* **482**, 72–76 (2012).
17. Tarakanova, A. & Buehler, M. J. The role of capture spiral silk properties in the diversification of orb webs. *J. R. Soc. Interface* **9**, 3240–3248 (2012).
18. Zhang, J., Rajkhowa, R., Li, J. L., Liu, X. Y. & Wang, X. G. Silkworm cocoon as natural material and structure for thermal insulation. *Mater. Design* **49**, 842–849 (2013).
19. Bejan, A. *Entropy generation minimization: the method of thermodynamic optimization of finite-size systems and finite-time processes* (CRC Press, Boca Raton, 1996).
20. Bejan, A. The constructal law of organization in nature: tree shape flow and body size. *J. Exp. Biol.* **208**, 1677–1686 (2005).
21. Růžička, V. & Klimeš, L. Spider (Araneae) communities of scree slopes in the Czech Republic. *J. Arachn.* **33**, 280–289 (2005).
22. Culver, D. C. & Pipan, T. Superficial subterranean habitats – gateway to the subterranean realm?. *Cave and Karst Science* **35**, 5–12 (2009).
23. Culver, D. C. & Pipan, T. *Shallow subterranean habitats* (Oxford University Press, Oxford, 2014).
24. Bejan, A. *Advanced engineering thermodynamics* [3rd ed.] (John Wiley & Sons, Hoboken, 2006).
25. Bejan, A. & Lorente, S. The constructal law and the evolution of design in nature. *Phys. Life Rev.* **8**, 209–240 (2011).
26. Decou-Burghele, A. Sur la biologie de *Megaselia melanocephala* von Roser, Phoride parasite des cocons de *Meta menardi* latr. *Annal. Lab. Souterrain Hansur-Lesse* **11**, 16–22 (1961).
27. Austin, A. D. The function of spider egg sacs in relation to parasitoids and predators, with special reference to the Australian fauna. *J. Natur. Hist.* **19**, 359–376 (1985).
28. Novak, T. *et al.* Niche partitioning in orbweaving spiders *Meta Menardi* and *Metellina merianae* (Tetragnathidae). *Acta Oecologica* **36**, 522–529 (2010).
29. Zuur, A. F., Ieno, E. N. & Elphick, C. S. A protocol for data exploration to avoid common statistical problems. *Methods in Ecology & Evolution* **1**, 3–14 (2010).
30. Zuur, A. F., Ieno, E. N., Walker, N. J., Saveliev, A. A. & Smith, G. M. *Mixed effect models and extensions in ecology with R* (Springer, New York, 2009).
31. Foelix, R. F. *Biology of spiders* [2nd ed.] (Oxford University Press, Oxford, 1996).
32. Badino, G. Clouds in caves. *SEKA*, **2**, 1–8 (2004).
33. Isaia, M. *et al.* Aracnidi sotterranei delle Alpi Occidentali italiane (Arachnida: Araneae, Opiliones, Palpigradi, Pseudoscorpiones)/*Subterranean arachnids of the western Italian Alps (Arachnida: Araneae, Opiliones, Palpigradi, Pseudoscorpiones)* (Monografie XLVII. Museo Regionale di Scienze Naturali di Torino, 2011).
34. R Development Core Team. *R: a language and environment for statistical computing* (R Foundation For Statistical Computing, 2012).
35. Bird, R. B. & Lightfoot, E. N. *Transport phenomena* [2nd ed.] (John Wiley & Sons, New York, 2001).
36. Dobson, A. J. *An introduction to generalized linear models* (Chapman and Hall, New York, 1990).
37. Hurvich, C. M. & Tsai, C. L. Regression and time series model selection in small samples. *Biometrika* **76**, 297–307 (1989).
38. Burnham, K. P. & Anderson, D. R. *Model selection and multimodel inference: a practical information-theoretic approach* [2nd ed.](Springer-Verlag, New York, 2002).
39. Bartoń, K. *MuMIn: Multi-model inference.* (2013) Available at: http://CRAN.R-project.org/package=MuMIn. (Accessed:: 29th April 2014).
40. Neinhuis, C. & Barthlott, W. Characterization and distribution of water-repellent, self-cleaning plant surfaces. *Ann. Bot.* **79**, 667–677 (1997).
41. Lepore, E. & Pugno, N. Superhydrophobic polystyrene by direct copy of a lotus leaf. *Bionanoscience* **1**, 136–143 (2011).
42. Jeevananda, R. S. Simple formulae for the estimation of wet bulb temperature and precipitable water. *Indian J. Met. Hydr. Geophys.* **27**, 63–166 (1976).
43. Clift, R., Grace, J. R. & Weber, M. E. *Bubbles, drops, and particles* (Academic Press, 1978).

Acknowledgments

The authors would like to thank "Nanofacility Piemonte", INRIM Institute, for the FESEM microscope facility. EC and PA acknowledge the support of the Italian Ministry of Research (FIRB grant RBFR10VZUG). The *in-field* data were collected in the frame of CAVELAB "From microclimate to climate change: caves as laboratories for the study of the effects of temperature on ecosystems and biodiversity", a project funded by Compagnia di San Paolo and University of Torino (Progetti di Ateneo 2011, Cod. ORTO11T92F). NMP is supported by the European Research Council (ERC StG Ideas 2011 BIHSNAM n. 279985 on "Bio-Inspired hierarchical super-nanomaterials", ERC PoC 2013-1 REPLICA2 n. 619448 on "Large-area replication of biological anti-adhesive nanosurfaces", ERC PoC 2013-2 KNOTOUGH n. 632277 on "Super-tough knotted fibres"), by the European Commission under the Graphene Flagship (WP10 "Nanocomposites", n. 604391) and by the Provincia Autonoma di Trento ("Graphene Nanocomposites", n. S116/2012-242637 and reg.delib. n. 2266).

Author contributions

E.C. and P.A. suggested and developed the E-G-M- approach and designed the experimental laboratory measurements, M.I. and S.M. collected *in-field* data, analysed them with the related statistical models and provided biological arguments, E.L. performed SEM analysis, L.V. conducted laboratory experiments, N.M.P. designed and supervise this research and suggested the type of models. All the authors contributed to the writing of the paper and to the data analysis.

Additional information

Supplementary information accompanies this paper at http://www.nature.com/scientificreports

Competing financial interests: The authors declare no competing financial interests.

How to cite this article: Chiavazzo, E. *et al.* Cave spiders choose optimal environmental factors with respect to the generated entropy when laying their cocoon. *Sci. Rep.* **5**, 7611; DOI:10.1038/srep07611 (2015).

Supplementary Information for

Cave spiders choose optimal environmental factors with respect to the generated entropy when laying their cocoon

Eliodoro Chiavazzo[1], Marco Isaia[2], Stefano Mammola[2], Emiliano Lepore[3], Luigi Ventola[1], Pietro Asinari[1] & Nicola Pugno[3, 4, 5, *]

[1] Multi-Scale Modeling Lab (SMaLL), Department of Energy, Politecnico di Torino, Corso Duca degli Abruzzi 24, 10129 Torino, Italy.

[2] Laboratory of Terrestrial Ecosystems, Department of Life Sciences and Systems Biology, University of Torino, Via Accademia Albertina 13, 10123 Torino, Italy.

[3] Laboratory of Bio-inspired & Graphene Nanomechanics, Department of Civil, Environmental and Mechanical Engineering, University of Trento, Via Mesiano 77, 38123 Trento, Italy.

[4] Centre of Materials and Microsystems, Bruno Kessler Foundation, Via Santa Croce 77, 38122 Trento, Italy.

[5] School of Engineering and Materials Science, Queen Mary University, Mile End Rd, London E1 4NS, UK.

[*]Corresponding author: nicola.pugno@unitn.it

SUPPLEMENTARY FIGURES

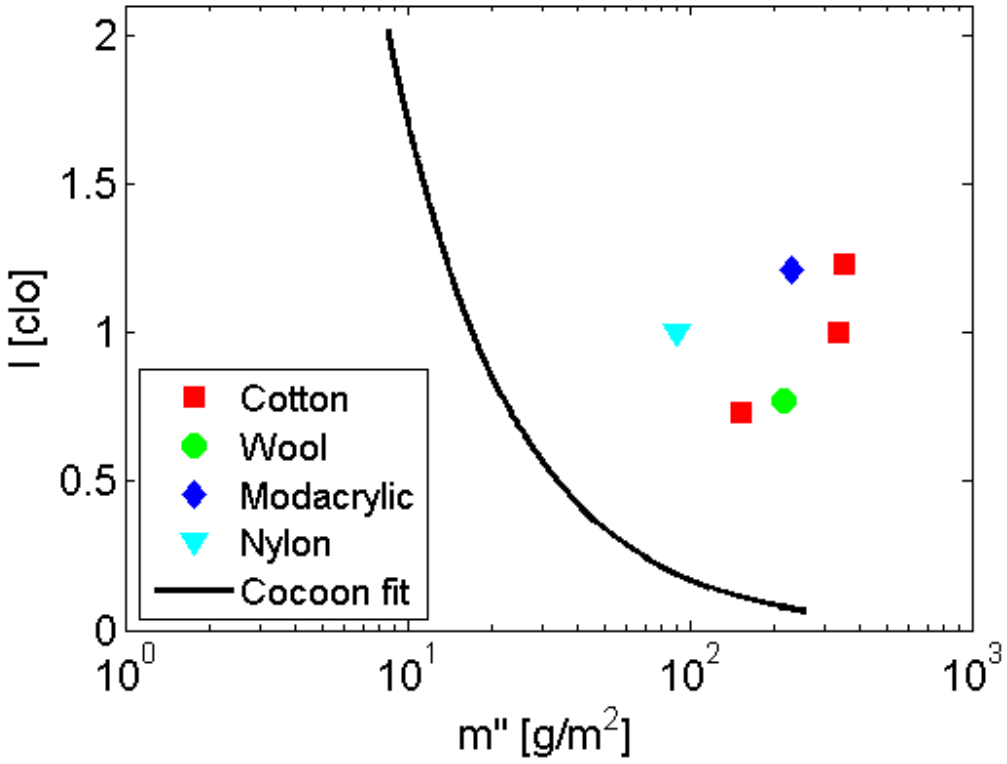

Supplementary Figure 1. Thermal insulation properties of cocoons. The cocoon silk is characterized by good thermal insulation properties and ultra-low weight as compared to traditional textiles. Here, the cocoon silk insulating properties are compared to those of traditional textiles. The specific weight (i.e. the weight per unit of insulation surface area, [g/m2]) is denoted by m'', while thermal insulation properties are measured in [clo] (1 clo = 0.155 m2K/W). For defining that quantity, the inner or the outer surface should be chosen. However, owing to the complex structure made of silk wires, the inner surface of a cocoon remains not clearly defined. To overcome these difficulties, we report the continuous black curve denoting the locus of all points of the the cocoon thermal performances corresponding to a range of insulation surfaces from a minimum value strictly needed to surround the eggs up to the maximum value (i.e. area of the outer surface). The black curve presents a hyperbolic shape as the thermal insulation quality and specific weight are directly and inversely proportional to insulation surface area, respectively. Results show that cocoon silk might possibly significantly outperform the traditional textiles in terms of insulation properties (up to 2 times) and specific weight (up to 1 order of magnitude). In light of the above evidence, it is

reasonable to expect that those unusual thermal insulation properties may be replicated in the near future using the latest and most advanced manufacturing techniques. To this end, complex structures similar to those shown in the Figure 1a-e could be mimicked by means of 3D printing as soon as the necessary resolution requirements are met.

SUPPLEMENTARY NOTES

Supplementary Note 1. Study sites. Balma Fumarella (cadastre number: 1597 Pi/TO) is a small limestone cave, with a planimetric development of 47 m and a vertical ascent of 16 m. The entrance measures 2 x 2.5 m. The first hall of the cave (approximately 2 x 3 x 20 m) is followed by a narrow passage and a second hall of approximately 1 x 2 x 10 m. In the inner part of the cave the mean annual temperature is around 11 °C (measured at ground level).

Cave di Marra (cadastre number: art. Pi/TO) is an abandoned mine of gneiss. The mine is basically a long tunnel of nearly 70 m, with a regular section of 4 x 5 m. The entrance connecting the tunnel to the outside is a quadrangular hole measuring 1.5 x 2 m. The mean annual temperature inside the tunnel is around 9 °C (measured at ground level).

Grotta del Bandito (cadastre number: 1002 Pi/CN) is a limestone cave, with a labyrinthine planimetric development of 336 m and a vertical ascent of 7 m. The main entrance of the cave measures around 1.5 x 2.5 m and is followed by a 35 m tunnel, with a section of 2.5 x 4 m. A minor entrance (1.5 x 1.5 m) is followed by a narrow tunnel of 10 m leading to a small chamber of approximately 4 x 3 x 10. The mean annual temperature inside the cave is around 10 °C (measured at ground level).

Supplementary Note 2. Model validation. In order to investigate the existence of a possible non-linear response between the presence/absence of cocoons and the explanatory variables, we applied a generalized additive mixed model (GAMM) that allowed us to fit a non-linear effect (smooth) of the covariates on the dependent variable. The model was fitted via the mgcv[1] R package (version 1.7-27) with the same structure derived from the previous model selection. The non-linear trend was rejected by plotting the smooth of the covariates against the observations, revealing a clear linear pattern and confirming the validity of the estimate values generated by the linear mixed model.

Supplementary Note 3. Laboratory experiments. A heater consisting of a compact and thermally stable electrical resistance (of value R) is inserted within the spider cocoon and supplied with a constant potential V. The thermal transmittance Tr can thus be calculated as follows:

$$Tr = \frac{\dot{Q}}{T_w - T_a} = \frac{\frac{V^2}{R}}{T_w - T_a}, \qquad (1)$$

where T_w and T_a are the temperature values recorded by a thermocouple in contact with the above heater and the air temperature, respectively.

Moreover, in our analysis, we also investigated the mass transfer and characteristic times governing the drying and wetting phenomena of the cocoon surface. Let us suppose that a cocoon (initially at a temperature T_w) is sprayed with water by a nozzle ensuring uniform wetting of the entire surface, and concurrently it is invested by an airflow at temperature T_a, velocity U_{air} and relative humidity φ.

In natural conditions, we expect that the cocoon surface experiences several partial wetting events during the time of egg presence. Here, for simplicity, we only considered a single complete wetting event, assuming this is representative of the several natural events.

The partial pressure of water vapor on the cocoon surface is the saturation pressure at T_w, $p_c = p_s(T_w)$, while the partial pressure of water vapor within the air stream is $p_a = \varphi p_s(T_a)$. Assuming $T_w > T_a$, this implies $p_c > p_a$. Thus, a vapor pressure difference is established at the cocoon boundary. Such a difference is responsible for the water mass transport from the cocoon to the air. However, the water transport is possible upon vaporization, and the heat h_{vap} necessary for this process must be extracted from the cocoon itself, which consequently cools down (adiabatic cooling).

In general, the total heat power $\dot{Q}_{tot}$ flowing from the cocoon to the air is the sum of the convective heat flux $\dot{Q}_c$, dictated by the temperature difference, and the latent heat flux $\dot{Q}_{lat}$, which is proportional to the vapor pressure difference:

$$\dot{Q}_{tot} = \dot{Q}_c + \dot{Q}_{lat} \qquad (2)$$

where $\dot{Q}_c = Tr\left(T_w - T_a\right)$ and $\dot{Q}_{lat} = h_{vap} K\left[p_s\left(T_w\right) - \varphi p_s\left(T_a\right)\right]$, being Tr and K the thermal and mass transport transmittance, respectively. During the first set of experiments, we only measured the thermal transmittance Tr, while the mass transport transmittance K was derived by invoking the Chilton-Colburn analogy[2].

In a second set of experiments, in order to determine the characteristic drying time, we focused on a fast wetting process of the cocoon followed by the subsequent drying due to forced airflow. In particular, the cocoon became wet by a spray nozzle, where water is constantly kept thermostatted at the ambient temperature T_a, and the cocoon itself is in thermal equilibrium with airflow before getting wet (see also the Fig. 2 in the main text). At this time, the heater is not powered and no heat sources are present in the cocoon, so that the temperature inside the cocoon suddenly decreases due to adiabatic cooling. Consequently, the temperature T_w decreases generating a temperature difference, and consequently a convective heat flux from the air to the cocoon. To summarize, a heat flux $\dot{Q}_c$ is observed from the air to the cocoon, while a latent (or vaporization) heat flux $\dot{Q}_{lat}$ goes from the cocoon to the air.

More specifically, the temperature T_w varies during time: starting from the initial value $T_w\left(t = 0\right) = T_a$, we firstly observe a sudden temperature decrease till a minimum value is reached (since T_a is constant, $\Delta T = T_a - \left(T_w\right)_{\min} = \Delta T_{\max}$), and subsequently an increase towards the initial value T_a.

We performed experiments exploring different value of the air velocity U_{air} . For each experiment, we calculate the drying constant time, defined as:

$$\tau = t_{tau} - t_{start} \quad (5)$$

where t_{start} indicates the time instant when the cocoon is sprayed, while t_{tau} is the characteristic time, such that $T_a - T_w(t = \tau) = (1 - 0.63)\Delta T_{\max}$.

Supplementary Note 4. Characterization of heat and mass transport transmittances.

During the first set of tests in the wind channel, the electrical assembly (heater and thermocouple described above. See also the Methods section in the main manuscript) is initially characterized without being surrounded by a cocoon (below referred to as naked setup). Subsequently, the above assembly is introduced within the cocoon, and the same characterization is performed.

The error bars in Figure 4a (main manuscript) represent the confidence interval at a level of 95%. Here, two kinds of measurement uncertainties are taken into account: type A uncertainties based on statistical analysis of measured quantities, and type B uncertainties determined by means of any other information (e.g. datasheets).

In this first set of experiments, measurements showed a good repeatability. Therefore, type B uncertainties were judged enough to construct the desired confidence interval. Equation (1) is used to compute Tr as a function of other measured quantities (V, T_a, T_w) and parameters (R), hence $Tr = Tr(V, T_a, T_w, R)$. The standard uncertainty σ_{Tr} for the quantity Tr can be computed by the following formula[3]

$$\sigma_{Tr} = \sqrt{\sum_{i=1}^{4} \sigma_{q_i} \frac{\partial Tr}{\partial q_i}}, \quad (6)$$

where σ_{q_i} is the standard uncertainty for the i-th independent quantity $q_i \in (V, T_a, T_w, R)$.

Supplementary Note 5. Dimensionless analysis. Since analytical solutions are not available for the majority of thermal fluid dynamics problems, it proves convenient to identify all relevant dimensionless quantities governing a system of interest, and ultimately obtain a correlation to relate those quantities.

Except for experiments at an airflow velocity of 0 m/s, here we deal with forced convective heat transfer on a body (naked heaters and cocoons). Hence, two dimensionless numbers are known to be relevant for such systems: the first one is the Reynolds number (Re), defined as:

$$Re = \frac{\rho_a U_{air} L_c}{\mu}, \qquad (7)$$

where ρ_a is the density of the fluid, U_{air} is the airflow velocity, L_c is a characteristic length and μ is the dynamic viscosity. The characteristic length is different for each type of flow. For naked configurations, L_c is chosen to be the height of the cylindrical heater, while in the presence of cocoons it is the square root of the external surface S_c of the cocoon $L_c = \sqrt{S_c}$.

The second relevant dimensionless quantity is the Nusselt number (Nu), defined as:

$$Nu = \frac{hL_c}{\lambda} = \frac{TrL_c}{S\lambda} \qquad (8)$$

where λ is the thermal conductivity of the fluid, L_c is a characteristic length (chosen as described above) and h is the convective heat transfer coefficient, obtained as the ratio between the transmittance Tr and the external surface S of the body.

Supplementary Note 6. Characterization of mass transport properties of *Meta menardi* cocoons and the influence of humidity. We considered that the surface through which the mass

transfer occurs presents the same area as the one through which convective heat transfer happens. Such an assumption, combined with the Chilton-Colburn analogy between heat and mass transfer phenomena[2], allow us to state the following relationship:

$$Tr = Tr\left(U_{air}\right) = Tr_0 + Tr_1 U_{air}^{\alpha} \qquad (9)$$

which implies:

$$K = K\left(U_{air}\right) = K_0 + K_1 U_{air}^{\alpha}\ , \qquad (10)$$

hence:

$$\frac{K_0}{Tr_0} = \frac{K_1}{Tr_1} = \frac{T_a - T_{wb}}{h_{vap}\left[p_s\left(T_{wb}\right) - \varphi p_s\left(T_a\right)\right]}\ , \qquad (11)$$

where T_{wb} is the wet bulb temperature corresponding to the ambient relative humidity φ and ambient temperature T_a, as measured during our experiments. The quantities Tr_0, Tr_1 and α in (9) are chosen to best-fit the experimental data, while K_0 and K_1 are the corresponding parameters in the equation for the mass transport transmittance (10). Thus, based on the experiments in Figure 4a (main manuscript), the mass transport transmittance K is fully determined thanks to the latter equation (11), and results are reported in Figure 4c (main manuscript).

Moreover, the wetting experiments have been performed in order to estimate the characteristic drying time τ as a function of the airflow velocity U_{air}. Results are shown in Figure 4d (main manuscript).

The error bars in Figure 4d represent the confidence interval at a level of 95%. To construct a confidence interval in this case both type A and type B uncertainties should be taken into account, due to a poorer repeatability (compared to measurements in Figure 4a) of the experimental measurements of τ. Thus, for each airflow velocity value a significant number of experiments have

been done, and then type A uncertainties $\sigma_{\tau,A}$ have been calculated using both t-student and chi-squared methods. Type B uncertainties have been calculated as in the case of Tr , where τ was regarded as a function of three independent quantities $\left(time, T_w, T_a\right)$, and the overall uncertainty is calculated as:

$$\sigma_\tau = \sqrt{\sigma_{\tau,A}^2 + \sigma_{\tau,B}^2} \,. \qquad (12)$$

SUPPLEMENTARY REFERENCES

1. Wood, S. N. Generalized additive models: an introduction with R (Chapman & Hall/CRC, 2006).

2. Bird, R. B. & Lightfoot, E. N. (2nd edition). Transport phenomena (John Wiley & Sons, 2001).

3. Kline, S. J. & McClintock, F. A. Describing uncertainties single-sample experiments. Mech. Eng. 75, 38 (1953).